ACS MEASUREMENT SCIENCE Au
AN OPEN ACCESS JOURNAL OF THE AMERICAN CHEMICAL SOCIETY

pubs.acs.org/measureau

Article

Combining Micropunch Histology and Multidimensional Lipidomic Measurements for In-Depth Tissue Mapping

Melanie T. Odenkirk, Brian M. Horman, James N. Dodds, Heather B. Patisaul, and Erin S. Baker*

Cite This: ACS Meas. Sci. Au 2022, 2, 67–75

Read Online

ACCESS | Metrics & More | Article Recommendations | Supporting Information

ABSTRACT: While decades of technical and analytical advancements have been utilized to discover novel lipid species, increase speciation, and evaluate localized lipid dysregulation at subtissue, cellular, and subcellular levels, many challenges still exist. One limitation is that the acquisition of both in-depth spatial information and comprehensive lipid speciation is extremely difficult, especially when biological material is limited or lipids are at low abundance. In neuroscience, for example, it is often desired to focus on only one brain region or subregion, which can be well under a square millimeter for rodents. Herein, we evaluate a micropunch histology method where cortical brain tissue at 2.0, 1.25, 1.0, 0.75, 0.5, and 0.25 mm diameter sizes and 1 mm depth was collected and analyzed with multidimensional liquid chromatography, ion mobility spectrometry, collision induced dissociation, and mass spectrometry (LC-IMS-CID-MS) measurements. Lipid extraction was optimized for the small sample sizes, and assessment of lipidome coverage for the 2.0 to 0.25 mm diameter sizes showed a decline from 304 to 198 lipid identifications as validated by all 4 analysis dimensions (~35% loss in coverage for ~88% less tissue). While losses were observed, the ~200 lipids and estimated 4630 neurons contained within the 0.25 punch still provided in-depth characterization of the small tissue region. Furthermore, while localization routinely achieved by mass spectrometry imaging (MSI) and single cell analyses is greater, this diameter is sufficiently small to isolate subcortical, hypothalamic, and other brain regions in adult rats, thereby increasing the coverage of lipids within relevant spatial windows without sacrificing speciation. Therefore, micropunch histology enables in-depth, region-specific lipid evaluations, an approach that will prove beneficial to a variety of lipidomic applications.

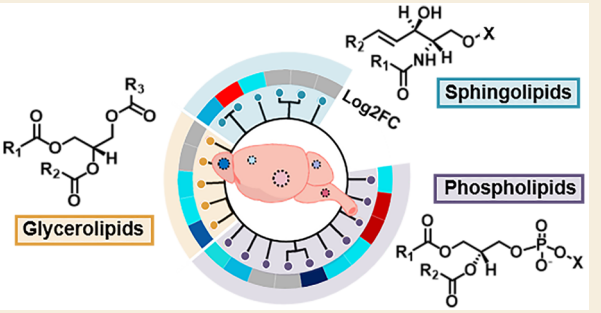

KEYWORDS: *Lipidomics, Tissue, Brain, Cortex, Mass spectrometry*

INTRODUCTION

Lipids represent a family of hydrophobic and amphipathic biomolecules that include fats, membrane lipids, signaling molecules, and hormone precursors.[1] The structural diversity of lipids provides flexible utility in a myriad of biological processes and region-specific expression across various tissue and cell types that is still being discovered. To date, more than 44 000 entries exist in the LIPID MAPS database with computational projections suggesting that 180 000 unique species comprise the entire lipidome.[2−4] Analytically, annotation of the 180 000 estimated lipids within the lipidome is a momentous challenge.[2] Mass spectrometry (MS) is a vastly popular method routinely implemented as a stand-alone, high-throughput means of assessing lipid perturbations through shotgun lipidomics.[5] However, the prevalence of isomeric species, discrepancies of ionization efficiency across distinct lipid classes, and dynamic range differences in lipid abundance within an organism deters the depth of lipidome annotation capable solely using MS. Liquid chromatography and ion mobility spectrometry in conjunction with MS (LC-IMS-MS) offer orthogonal dimensions of separation that mitigate the deconvolution of some overlapping signals for improved lipidome coverage and heightened identification confidence.[6,7] Additional methodologies for enhancing lipid separation have facilitated the differentiation of double bond and fatty acyl position isomers that heighten mechanistic insight at the cost of manual annotation.[8] As such, comprehensive lipidomics is still predominantly composed of LC-MS/MS workflows with the objective of providing vast lipidome coverage and detailed information on the structural moieties comprising individual lipid species. The recent discovery of novel lipid classes such as resolvins and neurofurans demonstrates the continued expansion of the annotated lipidome from LC-MS/MS.[9,10] These LC-MS/MS analyses, however, largely focus on homogenized tissue or serum and plasma samples, limiting

Received: September 6, 2021
Revised: October 13, 2021
Accepted: October 14, 2021
Published: October 28, 2021

https://doi.org/10.1021/acsmeasuresciau.1c00035
ACS Meas. Sci. Au 2022, 2, 67−75

analysis of localized lipid dysregulation across heterogeneous tissue. The brain, for example, is a complex organ with distinct functions across small anatomical regions.[11,12] In adult rodents, the cortical region, which is responsible for information processing, has distinct subregions for visual, auditory, and motor functions with tissue volumes below 5 mm^3.[13] Thus, other MS applications have emphasized the investigation of localized lipid dysregulation across complex tissue types.

Mass spectrometry imaging (MSI) has prioritized the investigation of localized dysregulation via the ablation of tissue that is then topographically mapped to structural defined areas.[14] Decades of MSI advancements have enhanced the spatial resolution of these applications to achieve pixel sizes as small as 1−5 μm, providing detailed localization of individual lipid species in tissues of an area equivalent to a singular cell.[15−17] The biggest caveat of MSI, however, is that localization often supersedes detailed speciation. For example, the lacking compatibility of imaging with sample preparation and front-end separations increases ambiguity in structural characterization, and the misalignment of MS and MS/MS spectra also challenges the parallel acquisition of both precursor and product ions for analyte identification.[14,18] To overcome the speciation challenges of traditional MSI, some researchers have adopted IMS for increasing identification confidence.[19,20] Nonetheless, most imaging workflows continue to rely on mass as the sole descriptor for making lipid identifications. The momentum of elucidating differences in localized lipid expression has further carried over to single cell research. Thus far, the emphasis of cell−cell heterogeneity within lipids has elucidated subclasses of neuronal and astrocyte cerebellar cells and genetic knockout and wild-type neurons.[21−23] However, the limited sampling material for both single cell and imaging workflows significantly impedes robust lipidome coverage. Single cell lipidomics average 37 abundantly expressed lipids for each cell, a figure approximately 10 times less than that of shotgun and comprehensive workflows.[21,22] From a practicality standpoint, single cell MS of the estimated 332 million cells in an adult rat brain is further complicated by the heterogeneous nature of biological tissue that impedes cell isolation in addition to throughput and data analysis.[24] Thus, it is clear that lipidomic experimental design often requires the sacrifice of either coverage or spatial information despite both factors providing meaningful insight into biology. However, interrogating lipid speciation and localized dysregulation across an organism's lipidome can facilitate biological knowledge of lipid dysregulation (Figure 1). Herein, we utilize LC-IMS-CID-MS (CID: collision induced dissociation) lipidomic analyses to investigate histological brain punches across 2.0 to 0.25 mm diameters and all at 1 mm depth. These multidimensional analyses provided increased lipid identification confidence, localization, and lipid speciation information. Additionally, we evaluated and optimized different lipid extraction methods for enhancing identifications with limited starting material.

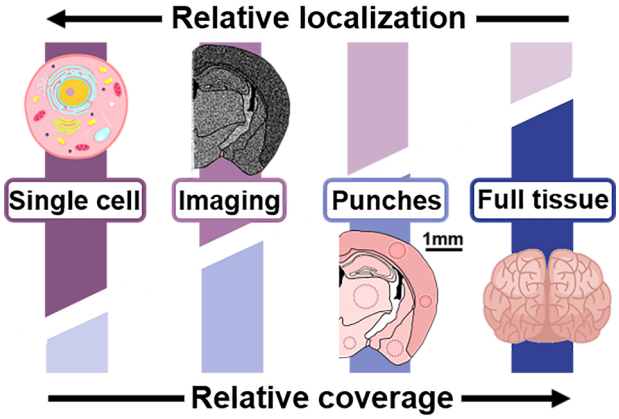

Figure 1. Lipidomic evaluations often create a trade-off between lipidome coverage and spatial information on lipid changes. Comprehensive LC-MS/MS workflows prioritize coverage, while single cell and imaging workflows favor detailed spatial information. Histology punches offer a means of achieving biologically relevant spatial information without significantly sacrificing speciation and coverage.

METHODS

Animal Care and Tissue Extraction

Brain micropunches were collected from three flash frozen, adult Wistar male rat brains at 2.0, 1.25, 1.0, 0.75, 0.5, and 0.25 mm diameters, using an approach routinely performed in neuroscience for over 30 years.[25,26] All punches were 1 mm in depth and were matched by cortical location for all animals. Animals (n = 3) were obtained from an existing colony housed in humidity- and temperature-controlled rooms at 22 °C and 30% average humidity, each with 12 h/12 h light/dark cycles (lights on at 6AM EST), following the Assessment and Accreditation of Laboratory Animal Care (AAALAC) approved Biological Resource Facility at NC State. Animal care, maintenance, and experimental protocols met the standards of the Animal Welfare Act and the U.S. Department of Health and Human Services "Guide for the Care and use of Laboratory Animals" and were approved by the NC State Institutional Animal Care and Use Committee (IACUC). The male rats were anesthetized with an overdose of CO_2 and then rapidly decapitated, and the brain was immediately removed, flash frozen on powdered dry ice, and stored at −80 °C until punch collection. Consistent with prior, similar work in the Patisaul lab, the brains were coronally cryosectioned until the anterior cingulate was exposed (approximately Bregma 1 mm).[26,27] One punch of each size was obtained from the cortex of each animal to yield a total of 3 punches per size. All punches were representative of the full cortical area which is largely homogeneous in terms of cell density. The punches were collected in SafeSeal Microcentrifuge tubes (Sorenson BioScience, Inc.) and transferred on dry ice to the Baker lab for analysis. Approximate neuron count was determined from the tissue volume and the average count of 92 600 neurons/mm^3 of cortex tissue (eq 1).[28]

$$\text{neuron count} = 92\,600\ \frac{\text{neurons}}{\text{mm}^3} \times \text{volume}\ (\text{mm}^3) \quad (1)$$

This equation illustrated an approximate neuron count range of 4630−291 000 across the 0.25 and 2.0 mm brain punches. While other cells such as astrocytes and glia exist in the cortex, for simplicity, only neuron numbers were estimated as these predominate the cortical region by approximately 2:1.[28]

Lipid Extraction

Lipid extraction performance was assessed through three facets: (i) effect of a 1 h incubation following organic phase addition, (ii) comparison of chloroform ($CHCl_3$) and methyl *tert*-butyl ether (MTBE), and (iii) reduced solvent volumes. For simplicity, the five extractions are referenced as Method 1 (M1), modified Folch;[29,30] Method 2 (M2), modified Folch with wait time; Method 3 (M3), modified Folch with wait time and reduced volume; Method 4 (M4), modified Matyash[31] with wait time; Method 5 (M5), modified Matyash with wait time and reduced volume. Detailed aliquot volumes and wait times for each extraction are provided in (Table 1). For reduced volume extractions (M3 and M5), the organic/H_2O/MeOH ratios of the Folch[30] and Matyash[31] extractions were kept constant relative to the original procedures which were previously

https://doi.org/10.1021/acsmeasuresciau.1c00035
ACS Meas. Sci. Au 2022, 2, 67−75

Table 1. Lipid Extraction Amounts for Folch (M1−M3) and MTBE (M4, M5) Extraction Procedures

	(A) Folch extraction						
	MeOH aliquot #1 (μL)	MeOH aliquot #2 (μL)	$CHCl_3$ aliquot (μL)	wait time (min)	H_2O aliquot #1 (μL)	H_2O aliquot #2 (μL)	total extraction time (h)[a]
method 1 (M1)	750	750	3000	0	200	1200	2.3
method 2 (M2), with wait time	750	750	3000	60	200	1200	3.3
method 3 (M3), with wait time and reduced volume	200	200	762	60	51	305	3.3
	(B) MTBE extraction						
	NH_4Ac aliquot (μL)	MeOH aliquot (μL)	MTBE aliquot (μL)	wait time (min)	H_2O aliquot (μL)	re-extraction volume (μL)	total extraction time (h)[a]
method 4 (M4), with wait time	200	1500	5000	60	1250	2000	2.0
method 5 (M5), with wait time and reduced volume	200	266	755	60	188	500	2.0

[a]The total extraction time sums all wait, centrifuge, vortex, sonication, and speedvac times.

optimized for lipid extraction.[32,33] Triplicate samples for each punch size were separately extracted and analyzed for a total of 90 samples (triplicate analysis of 5 extractions having 6 punch sizes and $n = 3$ for all 6 punch sizes assessed using M1).

Modified Folch[29,30] extraction method (M1−M3) samples were homogenized with the first aliquot of −20 °C methanol (M1 and M2:750 μL, M3:200 μL) in 2.0 mL, 2.4 mm tungsten-carbine bead tubes for 5 min with a Fisherbrand 24 bead mill. Another aliquot of methanol was added following sample transfer to glass vials with a Teflon-lined cap (M1 and M2) or 1.7 mL Sorenson BioScience tubes (M3) (Salt Lake City, UT).[30] Chloroform was subsequently added at a 2:1 ratio to total methanol. M2 and M3 samples were incubated for 1 h at room temperature prior to continuing the extraction procedure. Afterward, samples underwent a 30 s vortexing step before and after 30 min of sonication at room temperature. Samples were then left to incubate at 4 °C for 1 h following the addition of the first water aliquot (M1 and M2: 200 μL, M3: 51 μL). The second aliquot of water was added prior to centrifugation at 1000*g* for 10 min. Then 200 μL of the lower organic phase was dried via speedvac and subsequently reconstituted in 10 μL of $CHCl_3$ and 190 μL of MeOH for MS analysis.

The MTBE extraction protocol was adopted from Matyash et al.[31] for the M4 and M5 extractions. Samples were initially homogenized using identical bead homogenizer settings as above with a 200 μL aliquot of water with 0.1% ammonium acetate. Methanol was added to homogenized tissue, and samples were transferred to either glass vials with a Teflon-lined cap (M4) or Sorenson BioScience tubes (M5).[30] Samples were subsequently vortexed for 30 s and MTBE (M4: 5000 μL, M5: 755 μL) was introduced prior to 1 h incubation at room temperature. Water (M4: 1250 μL, M5: 188 μL) was subsequently added to induce phase separation, and samples were incubated for an additional 10 min at room temperature. Samples were then centrifuged at 1000*g* for 10 min, and the upper organic phase was collected. The lower phase was re-extracted with a 10:3:2.5 ratio of MTBE/MeOH/H_2O (M4: 2000 μL, M5: 500 μL). Organic phases were subsequently combined, and 200 μL aliquots were dried via speedvac and reconstituted in 10 μL $CHCl_3$ and 190 μL MeOH for LC-IMS-CID-MS analysis.

LC-IMS-CID-MS Analysis

An Agilent 1290 Infinity II UHPLC coupled to an Agilent 6560 IM-QTOF MS platform (Santa Clara, CA) was utilized for the analysis of 75 brain punch lipid extracts.[34,35] IMS-MS data was collected with both positive and negative ESI from 50 to 1700 m/z. A cycle time of 1 s/spectra was applied to intensify the signal of low abundant ions. Alternating scans of no fragmentation and all-ions data independent acquisition (DIA) were used to obtain both precursor and fragmentation information simultaneously as DDA acquisition requires modifications to the 6560 platform.[36] Collision energies for the collision-induced dissociation (CID) of lipids were ramped based on IMS drift times, providing optimized fragmentation for different ion sizes and charge states.[37,38] Injection volumes of 10 μL of each sample were chromatographically separated on a reversed phase Waters CSH column (3.0 mm × 150 mm × 1.7 μm particle size) over a 34 min gradient (MPA: ACN/H_2O (40:60) containing 10 mM NH_4Ac; MPB: ACN/IPA (10:90) containing 10 mM NH_4Ac) at a flow rate of 250 μL/min.[39] Detailed information on the gradient and column wash are provided in Supporting Information Table S1.

Lipid Identification, Statistics, and Analysis

From our LC-IMS-CID-MS platform, retention time, collisional cross section (CCS), and m/z values of both precursor and fragment ions were simultaneously collected. Lipid identifications were made in Skyline from a library developed in-house of 516 lipids with experimentally validated LC, IMS, and MS information.[40,41] Spectra were deconvoluted based on the alignment of fragment ions to precursor signals in LC and IMS dimensions which was determined to be sufficient for identifying individual lipids. The speciation of lipids commonly included the headgroup and fatty acyl (FA) assignments (i.e., PC(16:0_18:1)) without the annotation of double bond position, orientation, or the backbone position of FA connectivity.[3,8] For the 2.0 mm brain punch diameter, a total of 314 lipid signals were observed across positive and negative ionization modes.

To assess extraction performance, the $\log_2$ transformed positive and negative mode lipidomic data was assessed for outliers using RMD-PAV, Pearson correlation, and principal component analysis (PCA) in pmartR (version 0.9).[42] Samples that failed outlier tests and lipids lacking data for relative quantitation were removed from the data set. Total ion current (TIC) normalization was then applied in MetaboAnalyst (version 4.0).[43] To assess extraction performance, the relative abundance of individual lipid species across each pairwise comparison was assessed. The normalized, $\log_2$ transformed data underwent an ANOVA with an $\alpha = 0.05$ and a Holm correction in pmartR.[42] Normalized abundances and statistical outputs for (a) modified Folch with and without wait times (M2 vs M1), (b) MTBE and Folch comparisons (M4 vs M2), and (c) reduced volumes of modified Folch (M3 vs M2) and MTBE extractions (M5 vs M4) for all brain punches are presented in Tables S2−S7. Data outputs were visually summarized with the SCOPE toolbox to cluster lipids by structural relationships in R.[44−49] Fold change outputs from the statistical analysis were then overlaid to illustrate trends in statistically upregulated (red), downregulated (blue), and not significant (gray) lipid species.

RESULTS AND DISCUSSION

Optimizing Brain Punch Extractions

Despite the brain being the second most lipid rich region of the body, with adipose tissue being the first, the limited quantity of material for MS analysis can hinder lipidome coverage.[50] Therefore, the first objective of this research was to expand on comparisons of lipid extraction efficiency with a range of sample amounts.[32,51] Established workflows of Folch[29]

https://doi.org/10.1021/acsmeasuresciau.1c00035
ACS Meas. Sci. Au 2022, 2, 67−75

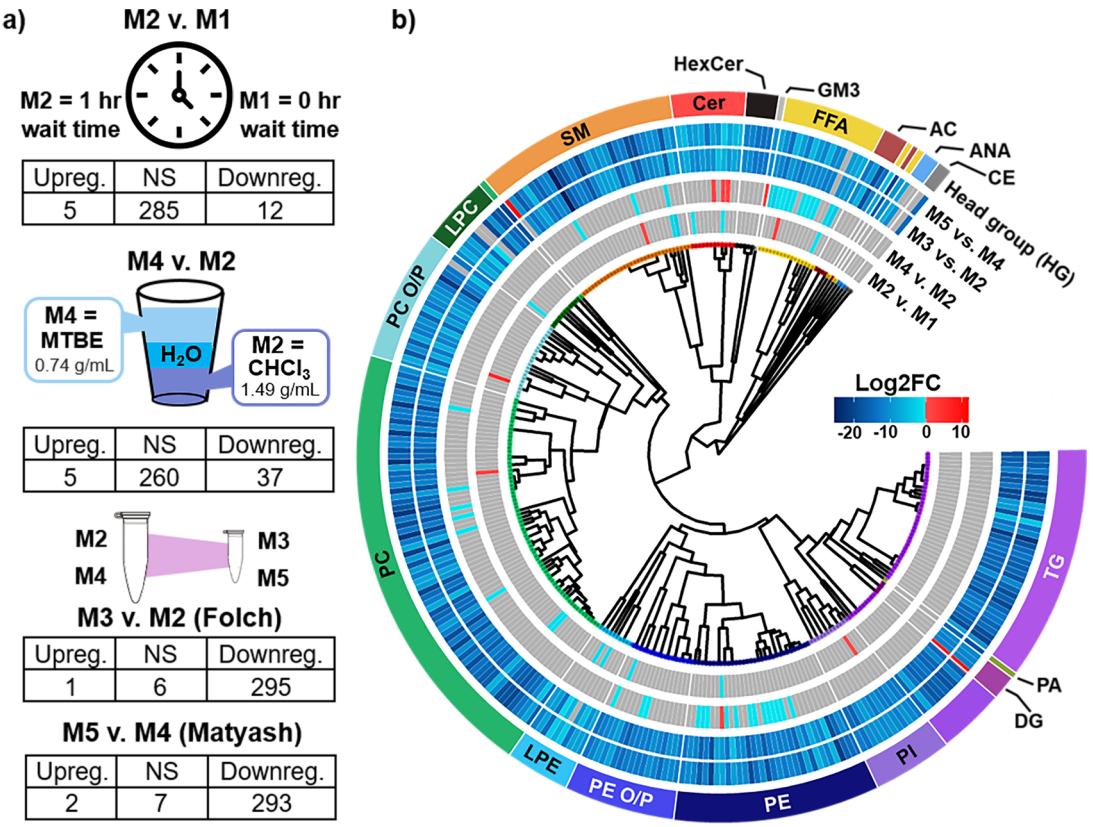

Figure 2. Lipid extraction method comparison. (a) Tables of significant lipids for 1.25 mm punch diameters showing Folch extraction efficiency (Folch vs Folch with wait; M2 vs M1), Matyash and Folch extraction efficiency (Folch vs Matyash; M4 vs M2), and comparison of reducing extraction volumes for Folch (M3 vs M2) and Matyash (M5 vs M4) extractions. (b) Circular dendrogram of all 302 lipids signals was generated with an ECFP_6 fingerprint, Tanimoto distance, and average linkage for the corresponding extraction method comparisons. Log_2FC is overlaid for all three comparisons to visualize trends in significant dysregulation. All identified but insignificant lipids are shown in gray, whereas statistically significant species that were either upregulated or downregulated are displayed in red and blue.

and Matyash[31] extractions were modified to include (1) a 1 h wait time following organic solvent addition, (2) comparison of MTBE and $CHCl_3$ as organic solvents, and (3) reduction of extraction volume amounts (Figure 2a). These three variables were chosen to optimize lipidome extraction through complementary facets. Wait times following organic solvent addition, for example, have previously been applied to facilitate the diffusion of lipids into the organic phase in mammalian tissue.[52] Organic solvents and their respective ratios have been assessed for optimizing lipid extraction protocols with comparable performances, but prior work has not considered organic solvent extraction efficiency with limited sampling material.[32,51] Finally, the reduction of extraction volumes was investigated to minimize sample transfer throughout extraction. Importantly, the ratio of solvent was kept consistent between original and reduced methods.[32,33] Overall, similar trends in lipid dysregulation were observed across brain punch sizes. Therefore, data from only the 1.25 mm brain punch diameter was used to consider the extraction efficiencies for each comparison (Figure 2b).

The hypothesis of an additional incubation period facilitating lipid partitioning into the organic layer was not supported as we observed little effect on lipid recovery between M1 and M2 (0 and 60 min, respectively). In this comparison, 12 lipids were found to be significantly downregulated and 5 were found to be upregulated of the 302 identifications. No trends of lipid category, class, or fatty acyl composition were observed for the significant species. Given that the additional incubation time has largely been applied for extraction of fibrous tissue types, the findings herein may suggest the effectiveness of lipid transfer to the organic phase from homogenized tissue is determined by tissue structure.[52]

MTBE and $CHCl_3$ are the most common organic solvents used for lipid extraction, and both solvents have been routinely assessed across a myriad of sample types demonstrating comparable performance across the major lipid classes.[32,33] Herein, a similar effect was observed where only 37 lipids were statistically downregulated and 5 were upregulated in the comparison of MTBE vs $CHCl_3$ (M4 vs M2). Notably, a number of dysregulated lipids in this comparison belonged to the free fatty acid (FFA) and phosphatidylethanolamine (PE) lipid classes. FFAs are known to partition between organic and aqueous layers during lipid extraction. The loss of FFA signals here contrasts with previous findings that MTBE facilitates better FFA recovery compared to chloroform.[31] When interpreting this result, it is important to emphasize FFA signals have many origins, including the degradation of complex lipid species, but this appears partially unsupported given the downregulation of complex lipids in MTBE vs $CHCl_3$. Instead, this observation may be an artifact of the use of methanol versus water during initial tissue homogenization as methanol facilitates the disruption of hydrogen bonding and hydrophobic interactions of the lipid bilayer.[32,33,52] Therefore, the observed downregulation of a number of membrane constituents and FFAs may reflect the significance of this initial step for improved lipid extraction. While these comparisons

https://doi.org/10.1021/acsmeasuresciau.1c00035
ACS Meas. Sci. Au 2022, 2, 67−75

showed a slight influence of an additional incubation period and organic solvents on lipid extraction, the reduction of solvent volumes for lipid extraction demonstrated a dramatic decrease of 97% of lipidome coverage for both Folch and Matyash procedures at a magnitude of $-20\log_2$FC despite a conservation of solvent ratios.[33] Notably, the sole upregulated lipid for both of these comparisons was DG(18:1_18:2), a potential decomposition product of more complex lipid species. The observations herein suggest that the most significant component of lipid extraction is the ratio of extraction volumes to sample material, as has been suggested by the work of Ulmer et al.[32] Altogether, the investigation of lipid extraction efficiency was relatively robust to solvent type and wait time but the best performance was observed following the modified Folch procedure (M1). Therefore, the following discussion of punch histology will focus on the results from this extraction.

Lipidome Coverage across Brain Punch Sizes

Following the selection of the modified Folch procedure (M1) for determining lipidome coverage across decreasing cell counts, all brain punch diameter sizes (2.0, 1.25, 1.0, 0.75, 0.5, and 0.25 mm) at 1.0 mm depth were analyzed with LC-IMS-CID-MS. To relate these to cell-based analyses, neuron numbers were estimated in each cortical punch size as this cell type is 2:1 to all other cell types within cortical brain tissue.[28] Estimated neuron cell counts ranged from 291 000 to 4630 for the 2.0 and 0.25 mm punch sizes, respectively (Figure 3a). The 2.0 mm diameter punches yielded a total of 179 and 135 identifications from positive and negative ionization modes based on experimentally validated CCS, m/z, fragment, and retention time values. The total 314 lipid identifications are also on par with other lipidomics experiments.[53] As punch size diminished, the number of lipid identifications also decreased over time from 314 to 302 to 295 to 278 to 248 and finally to 198 for the 0.25 mm diameter. While the decline in coverage was anticipated, a variation in slope was observed, with coverage being reasonably well conserved through 0.75 mm, and then a marked decrease was observed for the 0.5 and 0.25 mm punch diameters (Figure 3b). Relative to MSI, the corresponding area of the 0.25 mm punch size is 0.88 mm^2 which is approximately 3−4 times greater than the 250−200 μm spatial resolution capabilities of lower resolution imaging techniques which are often presliced to set the depth of spatial information.[14,54] However, prior work has estimated the total volume of the adult rat cortex to be 44 mm^3 with subcortex areas (i.e., auditory, motor, visual) falling within the range of 5−1.1 mm^3.[13] Therefore, the spatial isolation of all subcortical regions could readily be accomplished with brain punch diameters at or below 1 mm. This punch size corresponded to 165 positive mode and 130 negative mode lipid identifications, of which 28 were observed in both.

We next examined lipidome coverage losses to elucidate the missing identifications for each reduced punch diameter. In comparing the positive and negative ESI lipid losses for the 2.0 mm and the 0.25 mm diameters, we observed the depletion of lipids reflective of both poor ionization efficiency and low biological abundances as illustrated in the pie chart above each bar graph (Figure 3b). Triacylglycerol (TG, dark red), diacylglycerol (DG, red), and cholesterol ester (CE, pink) are all neutral molecules that are ionizable in positive ESI through adduction with an ammonium ion. Relative to phospholipid and sphingolipid species, this mechanism is far

a)

Brain punch diameter (mm)	2.0	1.25	1.0	0.75	0.5	0.25
Approximate neuron count	291,000	114,000	73,200	40,700	18,500	4,630
Brain punch area (mm^2)	12.6	6.4	4.7	3.2	2.0	0.9
Brain punch volume (mm^3)	3.14	1.23	0.79	0.44	0.20	0.05

b)

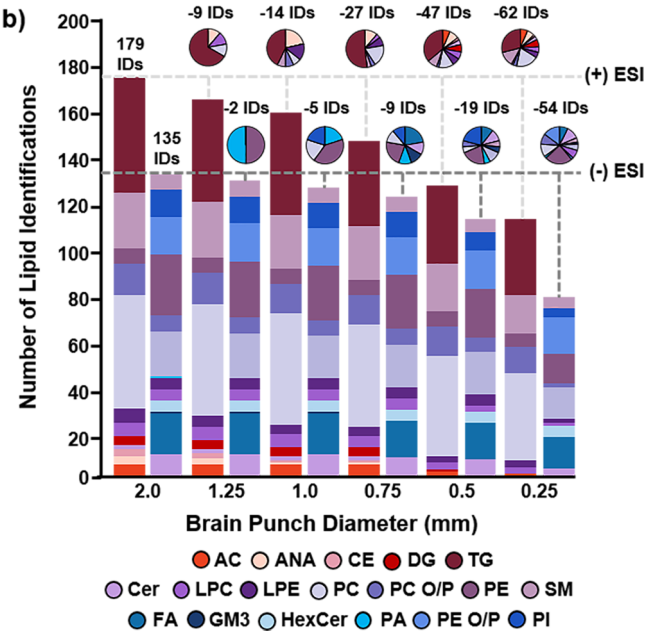

Figure 3. Brain lipidome coverage across punch sizes. (a) Each punch had a depth of 1.0 mm, and the diameters studied are shown in the table. Estimated neuron counts for each punch size are calculated using eq 1.[28] (b) Number of lipid species per class identified across brain punches in the positive and negative ion polarity analyses. A majority of lipid identifications lost in the smaller punch sizes were low abundant and/or less ionizable species.

less efficient and coelution of these species challenges the thorough annotation of these lipid classes.[55,56] Therefore, the high proportion of TG species lost with subsequently decreasing punch sizes and the absence of a CE signal below 0.75 mm is likely attributable to poor ionization in conjunction with reduced material. Taken together, the prevalence of neutral lipids annotated by positive ESI explains the steeper loss of lipids observed in positive mode relative to negative. Previous lipidome brain region analysis elucidated that phosphatidylcholine (PC), phosphatidylethanolamine (PE) , phosphatidylethanolamine alkyl ether/plasmalogen (PE O/P), phosphatidylserine (PS), hexose ceramide (HexCer), cholesterol (Chol), phosphatidylinositol (PI), and sphingomyelin (SM) classes make up 97% of the brain lipidome.[50] Individual, low abundance lipids belonging to these classes were lost with decreasing punch diameter. Additionally, entire lipid classes (phosphatidic acid (PA), acylcarnitine (AC), anandamide (ANA), ganglioside (GM3)) that constitute the remaining 3% of the lipidome were gradually unobserved with decreasing punch diameter, likely from the low abundance of these species within tissue. ANAs for example, are low-level lipids, with quantification estimates below 100 ng/mL in rat brain tissue that were no longer quantifiable below 0.5 mm punches.[57] Ceramides (Cer) are another class of lipids that constitute the remaining 3% of brain lipidome composition that was uniquely observed for all brain punches. Altogether, the lipidome

https://doi.org/10.1021/acsmeasuresciau.1c00035
ACS Meas. Sci. Au 2022, 2, 67−75

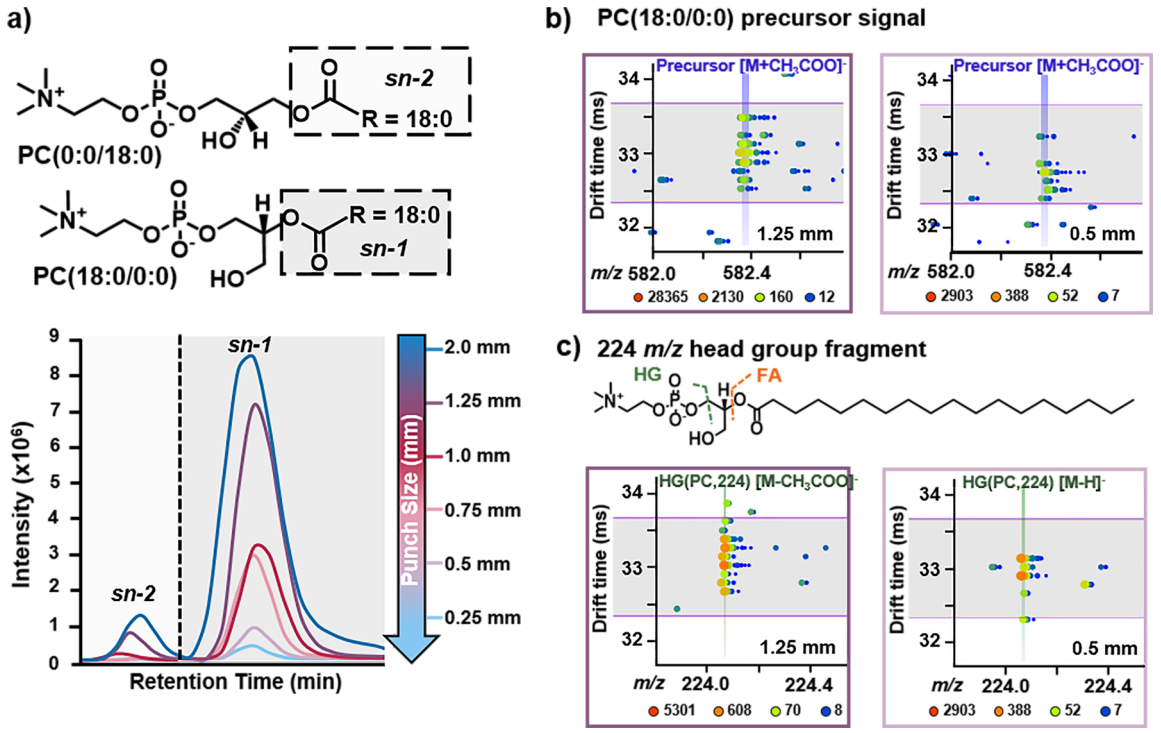

Figure 4. Signal abundance effects on lipid speciation. (a) Positive mode LC-IMS-MS/MS extracted ion chromatogram (EIC) of PC(0:0/18:0) and PC(18:0/0:0) across brain punches which are resolved by LC. (b) Drift spectra of the PC(0:0/18:0) precursor in negative ESI for 1.25 mm (left) and 0.5 mm (right). The decreased confidence in the *sn*-2 lipid presence also has greater implications on the speciation assignable for the more abundant *sn*-1 isomer. (c) CID fragment ion drift spectra in negative ESI for 1.25 mm (left) and 0.5 mm (right). The decreased intensity of the PC headgroup fragment ion at 0.5 mm decreases confidence in structural assignment. For both (b) and (c), the purple bars outline the region corresponding to the collisional drift time window of each ion determined by the instrument resolving power and analyte CCS.

coverage for the 0.25 mm punch size was composed of abundantly expressed lipids within the major classes with inclusion of lower level lipids as well. Given the loss of 88% of material relative to the 2.0 mm punch diameter, the retained 65% coverage of lipids for the 0.25 mm punch size suggests our histology method retained significant coverage. While some lipid differences are potential artifacts of micropunching across subregions of the cingulate cortex, no subregions were intentionally isolated. The consistent trend of lipid counts decreasing with punch size suggests this proof of concept is a robust depiction of micropunch capabilities and any effects of differential lipid expression across subregions is thought to be a minor contributing factor to the overall findings.

Brain Punch Diameter Effects on Lipid Speciation

The quality of lipid annotation through speciation capabilities is a crucial component for assessing lipidome coverage. CID fragmentation of lipids is diagnostic of the fatty acyl and headgroup moieties that constitute complex lipid structures.[55] Therefore, the simultaneous collection of precursor and fragment scans is of great importance for lipidomic experiments. The method deployed herein for CID fragmentation is a DIA all-ions approach where lipids in the same LC and IMS window are fragmented concurrently. Traditionally, in LC-MS applications, DIA fragmentation results in spectral complexity that can introduce ambiguity in assigning lipid identifications given the prevalence of shared structural motifs. IMS can assist in the deconvolution of complex fragmentation spectra by filtering signals in the drift time dimension.[37] Given the reproducibility of CCS values within 0.5% RSD, IMS is sufficient to deconvolute interfering signals for confident assignment of fatty acyl and headgroup constituents.[7,35,41] However, CID efficiency is variable based on ion mass, fragment type, and ionization mode.[58] Given the reduced number of ions reliably identified with decreasing abundance, annotation quality decreases as fragment ions are lost. The loss of 16:0 and 18:2 FA fragments, for example, reduces the annotation of a lipid from PC(16:0_18:2) to the summed fatty acyl PC(34:2) composition.[8] Biologically, this reduction in speciation is significant as the number of database matches increases from 12 to 30 potential structures.[3]

To explore how lipid speciation is influenced by decreasing brain punch size, we detail an example case of isomeric lipid separation by LC and the importance of fragmentation for lipid identification. The LC method leveraged within this study is slightly longer than other workflows to enhance lipid specificity at the expense of duty cycle.[39] Stereoposition isomers (*sn*-1 and *sn*-2) of lysophospholipids (LPLs) have a large enough difference in hydrophobicity that the order of LC elution varies such that the *sn*-2 lysophospholipid elutes prior to the *sn*-1 lysophospholipid. Therefore, we can confidently distinguish isomeric pairs such as PC(0:0/18:0) and PC(18:0/0:0) based on the LC elution order and slight shift in CCS values (Figure 4a). While the extracted ion chromatogram (EIC) ratio of these two conformers is conserved in the LC dimension, the abundance decreases with punch size. As punch sizes fall below 1.0 mm, the less abundant *sn*-2 PC(0:0/18:0) drops below the limit of detection even with drift time filtering (purple bar) as observed by comparing the signal in the nested drift spectra of the 1.25 mm punch size and 0.5 mm punch size of the precursor ion in Figure 4b. The stereochemical positioning of the fatty acyl depends heavily on the observation of two LC

https://doi.org/10.1021/acsmeasuresciau.1c00035
ACS Meas. Sci. Au 2022, 2, 67−75

peaks. Therefore, below 1.0 mm, this distinction becomes uncertain as the retention time differences used to differentiate these species could be attributed to slight experimental fluctuations. Thus, the speciation of this lipid decreases to PC(0:0_18:0) to denote this uncertainty.

Similar to how precursor abundance decreased with smaller punch sizes to limit the number of identifications, another critical component for assigning the FA composition of precursor signals is fragmentation data quality (Figure 4c). PC lipids are diagnostically annotated by the 224 and 184 m/z headgroup fragments observed from negative and positive ionization. While PC lipids are readily observed and quantified from the positive mode, structural fragmentation is less extensive compared to that of the negative mode due to reduced ionization for the fatty acyl groups.[55] Therefore, both negative mode and positive mode information is commonly evaluated for annotations and identifications. For the 1.25 mm punch size, the strong signal of the 224 PC headgroup fragment ion provides confident assignment of the corresponding m/z as a PC lipid. However, in the negative mode with the 0.5 mm diameter punch size, this signal diminishes such that it is indistinguishable from the noise. Therefore, the annotation of this lipid as a PC is ambiguous with the smaller punch and the 17 LIPID MAPS database matches corresponding to this feature cannot be further filtered to make a more specific annotation.[3] However, while fragmentation capabilities did decline with the reduction of sample size, potential annotations were still possible as performed with MSI but are not showcased in our reported numbers. Further, while the resolving power achieved with IMS is only ∼60, the deconvolution of spectra by drift time and retention time alignment facilitates the identification of lipid species.[59]

CONCLUSION

The simultaneous assessment of lipid speciation and location across an organism's lipidome is extremely difficult with existing analysis pipelines. Herein, we showcase the capabilities of combining micropunches and multidimensional LC-IMS-CID-MS analyses for the lipidomic assessment of brain tissue beginning with the optimization of lipid extraction for limited material. Extraction efficiency was determined to be robust across both wait time additions and organic solvents. Reduction of sample volumes, however, resulted in significant deterioration of lipidome annotation capabilities despite the conserved extraction ratios and removal of sample transfer steps with this method. Following the extraction analysis, lipidome coverage and speciation were both assessed by histological punch profiling. We observed that the signal losses of the initial 314 lipid identifications made from the 2.0 mm diameter punch to the 0.25 mm size occurred for the less abundant and poorly ionizable lipid classes. However, the 0.25 mm punch size still produced a robust coverage of 198 lipid species, an outcome that is particularly advantageous for neuroscientists because it is an optimal size for isolating and analyzing subcortical and other brain regions of interest in adult rat brains. Thus, micropunch histology can be a viable method for retaining coverage while simultaneously achieving meaningful spatial resolution to assess lipid dysregulation.

The final component of this investigation was the speciation of lipids analyzed with our LC-IMS-CID-MS platform. To provide confident headgroup and fatty acyl annotations, an abundant precursor signal is required for the complementary assessment of LC, IMS, and parent and fragment MS data. Here, we observed that speciation is also negatively influenced by reduced sample quantity as it was difficult to assign fragment ions for low abundance lipids. In conclusion, while losses were observed in the small punch diameters, this methodology was still able to annotate lipid headgroup and fatty acyls for approximately 200 lipids at punch sizes well below that of subcortex brain regions. Therefore, micropunch histology could significantly enhance the biological information achievable for lipidomic applications in small cellular or tissue-based samples collected from the brain or other organs.

ASSOCIATED CONTENT

Supporting Information

The Supporting Information is available free of charge at https://pubs.acs.org/doi/10.1021/acsmeasuresciau.1c00035.

LC elution and column re-equilibration method; statistical output for 2.0, 1.25, 1.0, 0.75, 0.5, and 0.25 mm diameter size brain punch comparison of extraction methods (XLSX)

AUTHOR INFORMATION

Corresponding Author

Erin S. Baker − *Department of Chemistry, North Carolina State University, Raleigh, North Carolina 27695, United States; Comparative Medicine Institute, North Carolina State University, Raleigh, North Carolina 27695, United States;* orcid.org/0000-0001-5246-2213; Email: ebaker@ncsu.edu

Authors

Melanie T. Odenkirk − *Department of Chemistry, North Carolina State University, Raleigh, North Carolina 27695, United States*

Brian M. Horman − *Department of Biological Sciences, North Carolina State University, Raleigh, North Carolina 27695, United States*

James N. Dodds − *Department of Chemistry, North Carolina State University, Raleigh, North Carolina 27695, United States;* orcid.org/0000-0002-9702-2294

Heather B. Patisaul − *Department of Biological Sciences and Center for Human Health and the Environment, North Carolina State University, Raleigh, North Carolina 27695, United States*

Complete contact information is available at: https://pubs.acs.org/10.1021/acsmeasuresciau.1c00035

Author Contributions

B.M.H. collected all brain punches. M.T.O. prepared, collected, and analyzed all data. The manuscript was written through contributions from all authors and the final version has been approved by all authors.

Notes

The authors declare no competing financial interest.

Raw data for this analysis is published on MassIVE (ftp://massive.ucsd.edu/MSV000088206/).

ACKNOWLEDGMENTS

This work was funded, in part, by grants from the National Institutes of Health (P30 ES025128, P42 ES027704, and P42 ES031009) and a cooperative agreement with the United

States Environmental Protection Agency (STAR RD 84003201). The views expressed in this manuscript do not reflect those of the funding agencies. The use of specific commercial products in this work does not constitute endorsement by the authors or the funding agencies. All LC-IMS-CID-MS measurements were made in the Molecular Education, Technology, and Research Innovation Center (METRIC) at NC State University.

ABBREVIATIONS

LC-IMS-CID-MS; liquid chromatography- ion mobility spectrometry-collision induced-mass spectrometr; MSI; mass spectrometry imaging; MS; mass spectrometry; IMS; ion mobility spectrometry; LC; liquid chromatography; LC-MS/MS; liquid chromatography-tandem mass spectrometry; $CHCl_3$; chloroform; MTBE; methyl *tert*-butyl ether; M1; modified Folch; M2; modified Folch with wait time; M3; modified Folch with wait time and reduced volume; M4; modified Matyash with wait time; M5; modified Matyash with wait time and reduced volume; MeOH; methanol; H_2O; water; IM-QTOF; ion mobility spectrometry-quadrupole time-of-flight; ESI; electrospray; DIA; data independent acquisition; DDA; data dependent acquisition; CID; collision induced dissociation; ACN; acetonitrile; IPA; isopropanol; NH4Ac; ammonium acetate; CCS; collisional cross section; FA; fatty acyl; FFA; free fatty acid; PE; phosphatidylethanolamine; DG; diacylglycerol; TG; triacylglycerol; CE; cholesterol ester; PC; phosphatidylcholine; PE O/P; phosphatidylethanolamine alkyl ether/plasmalogen; PS; phosphatidylserine; HexCer; hexose ceramide; Chol; cholesterol; PI; phosphatidylinositol; SM; sphingomyelin; PA; phosphatidic acid; AC; acylcarnitine; ANA; anandamides; GM3; ganglioside; Cer; ceramide; EIC; extracted ion chromatogram

REFERENCES

(1) Quehenberger, O.; Dennis, E. A. The Human Plasma Lipidome. *N. Engl. J. Med.* **2011**, *365* (19), 1812−1823.
(2) Yetukuri, L.; Ekroos, K.; Vidal-Puig, A.; Orešič, M. Informatics and Computational Strategies for the Study of Lipids. *Mol. BioSyst.* **2008**, *4* (2), 121−127.
(3) Liebisch, G.; Fahy, E.; Aoki, J.; Dennis, E. A.; Durand, T.; Ejsing, C. S.; Fedorova, M.; Feussner, I.; Griffiths, W. J.; Köfeler, H.; Merrill, A. H.; Murphy, R. C.; O'Donnell, V. B.; Oskolkova, O.; Subramaniam, S.; Wakelam, M. J. O.; Spener, F. Update on LIPID MAPS Classification, Nomenclature, and Shorthand Notation for MS-Derived Lipid Structures. *J. Lipid Res.* **2020**, *61* (12), 1539−1555.
(4) Fahy, E.; Subramaniam, S.; Murphy, R. C.; Nishijima, M.; Raetz, C. R. H.; Shimizu, T.; Spener, F.; van Meer, G.; Wakelam, M. J. O.; Dennis, E. A. Update of the LIPID MAPS Comprehensive Classification System for Lipids. *J. Lipid Res.* **2009**, *50*, S9−S14.
(5) Han, X.; Gross, R. W. Shotgun Lipidomics: Multidimensional MS Analysis of Cellular Lipidomes. *Expert Rev. Proteomics* **2005**, *2* (2), 253−264.
(6) Cajka, T.; Fiehn, O. Comprehensive Analysis of Lipids in Biological Systems by Liquid Chromatography-Mass Spectrometry. *TrAC, Trends Anal. Chem.* **2014**, *61*, 192−206.
(7) Paglia, G.; Angel, P.; Williams, J. P.; Richardson, K.; Olivos, H. J.; Thompson, J. W.; Menikarachchi, L.; Lai, S.; Walsh, C.; Moseley, A.; Plumb, R. S.; Grant, D. F.; Palsson, B. O.; Langridge, J.; Geromanos, S.; Astarita, G. Ion Mobility-Derived Collision Cross Section As an Additional Measure for Lipid Fingerprinting and Identification. *Anal. Chem.* **2015**, *87* (2), 1137−1144.
(8) Koelmel, J. P.; Ulmer, C. Z.; Jones, C. M.; Yost, R. A.; Bowden, J. A. Common Cases of Improper Lipid Annotation Using High-Resolution Tandem Mass Spectrometry Data and Corresponding Limitations in Biological Interpretation. *Biochim. Biophys. Acta, Mol. Cell Biol. Lipids* **2017**, *1862* (8), 766−770.
(9) Serhan, C. N.; Hong, S.; Gronert, K.; Colgan, S. P.; Devchand, P. R.; Mirick, G.; Moussignac, R.-L. Resolvins. *J. Exp. Med.* **2002**, *196* (8), 1025−1037.
(10) Song, W.-L.; Lawson, J. A.; Reilly, D.; Rokach, J.; Chang, C.-T.; Giasson, B.; FitzGerald, G. A. Neurofurans, Novel Indices of Oxidant Stress Derived from Docosahexaenoic Acid. *J. Biol. Chem.* **2008**, *283* (1), 6−16.
(11) Swanson, L. W. Brain Maps 4.0-Structure of the Rat Brain: An Open Access Atlas with Global Nervous System Nomenclature Ontology and Flatmaps. *J. Comp. Neurol.* **2018**, *526* (6), 935−943.
(12) Ma, Z.; Perez, P.; Ma, Z.; Liu, Y.; Hamilton, C.; Liang, Z.; Zhang, N. Functional Atlas of the Awake Rat Brain: A Neuroimaging Study of Rat Brain Specialization and Integration. *NeuroImage* **2018**, *170*, 95−112.
(13) Welniak-Kaminska, M.; Fiedorowicz, M.; Orzel, J.; Bogorodzki, P.; Modlinska, K.; Stryjek, R.; Chrzanowska, A.; Pisula, W.; Grieb, P. Volumes of Brain Structures in Captive Wild-Type and Laboratory Rats: 7T Magnetic Resonance in Vivo Automatic Atlas-Based Study. *PLoS One* **2019**, *14* (4), e0215348.
(14) Buchberger, A. R.; DeLaney, K.; Johnson, J.; Li, L. Mass Spectrometry Imaging: A Review of Emerging Advancements and Future Insights. *Anal. Chem.* **2018**, *90* (1), 240−265.
(15) Bowman, A. P.; Bogie, J. F. J.; Hendriks, J. J. A.; Haidar, M.; Belov, M.; Heeren, R. M. A.; Ellis, S. R. Evaluation of Lipid Coverage and High Spatial Resolution MALDI-Imaging Capabilities of Oversampling Combined with Laser Post-Ionisation. *Anal. Bioanal. Chem.* **2020**, *412* (10), 2277−2289.
(16) Lin, L.-E.; Chen, C.-L.; Huang, Y.-C.; Chung, H.-H.; Lin, C.-W.; Chen, K.-C.; Peng, Y.-J.; Ding, S.-T.; Wang, M.-Y.; Shen, T.-L.; Hsu, C.-C. Precision Biomarker Discovery Powered by Microscopy Image Fusion-Assisted High Spatial Resolution Ambient Ionization Mass Spectrometry Imaging. *Anal. Chim. Acta* **2020**, *1100*, 75−87.
(17) Kompauer, M.; Heiles, S.; Spengler, B. Atmospheric Pressure MALDI Mass Spectrometry Imaging of Tissues and Cells at 1.4-Mm Lateral Resolution. *Nat. Methods* **2017**, *14* (1), 90−96.
(18) Fisher, G. L.; Bruinen, A. L.; Ogrinc Potočnik, N.; Hammond, J. S.; Bryan, S. R.; Larson, P. E.; Heeren, R. M. A. A New Method and Mass Spectrometer Design for TOF-SIMS Parallel Imaging MS/MS. *Anal. Chem.* **2016**, *88* (12), 6433−6440.
(19) Paglia, G.; Kliman, M.; Astarita, G.; Claude, E.; Geromanos, S. Applications of Ion-Mobility Mass Spectrometry for Lipid Analysis. *Anal. Bioanal. Chem.* **2015**, *407*, 4995−5007.
(20) Woods, A. S.; Jackson, S. N. The Application and Potential of Ion Mobility Mass Spectrometry in Imaging MS with a Focus on Lipids. *Methods Mol. Biol.* **2010**, *656*, 99−111.
(21) Neumann, E. K.; Ellis, J. F.; Triplett, A. E.; Rubakhin, S. S.; Sweedler, J. V. Lipid Analysis of 30 000 Individual Rodent Cerebellar Cells Using High-Resolution Mass Spectrometry. *Anal. Chem.* **2019**, *91* (12), 7871−7878.
(22) Snowden, S. G.; Fernandes, H. J. R.; Kent, J.; Foskolou, S.; Tate, P.; Field, S. F.; Metzakopian, E.; Koulman, A. Development and Application of High-Throughput Single Cell Lipid Profiling: A Study of SNCA-A53T Human Dopamine Neurons. *iScience* **2020**, *23* (11), 101703.
(23) Evers, T. M. J.; Hochane, M.; Tans, S. J.; Heeren, R. M. A.; Semrau, S.; Nemes, P.; Mashaghi, A. Deciphering Metabolic Heterogeneity by Single-Cell Analysis. *Anal. Chem.* **2019**, *91* (21), 13314−13323.
(24) Herculano-Houzel, S. Isotropic Fractionator: A Simple, Rapid Method for the Quantification of Total Cell and Neuron Numbers in the Brain. *J. Neurosci.* **2005**, *25* (10), 2518−2521.
(25) Kim, K.; Jarry, H.; Knoke, I.; Seong, J. Y.; Leonhardt, S.; Wuttke, W. Competitive PCR for Quantitation of Gonadotropin-Releasing Hormone MRNA Level in a Single Micropunch of the Rat Preoptic Area. *Mol. Cell. Endocrinol.* **1993**, *97* (1−2), 153−158.
(26) Arambula, S. E.; Belcher, S. M.; Planchart, A.; Turner, S. D.; Patisaul, H. B. Impact of Low Dose Oral Exposure to Bisphenol A

https://doi.org/10.1021/acsmeasuresciau.1c00035
ACS Meas. Sci. Au 2022, 2, 67−75

(BPA) on the Neonatal Rat Hypothalamic and Hippocampal Transcriptome: A CLARITY-BPA Consortium Study. *Endocrinology* **2016**, *157* (10), 3856−3872.
(27) Arambula, S. E.; Jima, D.; Patisaul, H. B. Prenatal Bisphenol A (BPA) Exposure Alters the Transcriptome of the Neonate Rat Amygdala in a Sex-Specific Manner: A CLARITY-BPA Consortium Study. *NeuroToxicology* **2018**, *65*, 207−220.
(28) Keller, D.; Erö, C.; Markram, H. Cell Densities in the Mouse Brain: A Systematic Review. *Front. Neuroanat.* **2018**, *12*, 83.
(29) Folch, J.; Lees, M.; Stanley, G. H. S. A SIMPLE METHOD FOR THE ISOLATION AND PURIFICATION OF TOTAL LIPIDES FROM ANIMAL TISSUES. *J. Biol. Chem.* **1957**, *226* (1), 497−509.
(30) Nakayasu, E. S.; Nicora, C. D.; Sims, A. C.; Burnum-Johnson, K. E.; Kim, Y. M.; Kyle, J. E.; Matzke, M. M.; Shukla, A. K.; Chu, R. K.; Schepmoes, A. A.; Jacobs, J. M.; Baric, R. S.; Webb-Robertson, B. J.; Smith, R. D.; Metz, T. O. MPLEx: A Robust and Universal Protocol for Single-Sample Integrative Proteomic, Metabolomic, and Lipidomic Analyses. *mSystems* **2016**, *1* (3), 57343.
(31) Matyash, V.; Liebisch, G.; Kurzchalia, T. V.; Shevchenko, A.; Schwudke, D. Lipid Extraction by Methyl-Tert-Butyl Ether for High-Throughput Lipidomics. *J. Lipid Res.* **2008**, *49* (5), 1137−1146.
(32) Ulmer, C. Z.; Jones, C. M.; Yost, R. A.; Garrett, T. J.; Bowden, J. A. Optimization of Folch, Bligh-Dyer, and Matyash Sample-to-Extraction Solvent Ratios for Human Plasma-Based Lipidomics Studies. *Anal. Chim. Acta* **2018**, *1037*, 351−357.
(33) Christie, W. Preparation of Lipid Extracts from Tissues. In *Advances in Lipid Methodology*; Christie, W. W., Ed.; Oily Press: Dundee, 1993; Vol. *2*, pp 195−213.
(34) May, J. C.; Goodwin, C. R.; Lareau, N. M.; Leaptrot, K. L.; Morris, C. B.; Kurulugama, R. T.; Mordehai, A.; Klein, C.; Barry, W.; Darland, E.; Overney, G.; Imatani, K.; Stafford, G. C.; Fjeldsted, J. C.; McLean, J. A. Conformational Ordering of Biomolecules in the Gas Phase: Nitrogen Collision Cross Sections Measured on a Prototype High Resolution Drift Tube Ion Mobility-Mass Spectrometer. *Anal. Chem.* **2014**, *86* (4), 2107−2116.
(35) Stow, S. M.; Causon, T. J.; Zheng, X.; Kurulugama, R. T.; Mairinger, T.; May, J. C.; Rennie, E. E.; Baker, E. S.; Smith, R. D.; McLean, J. A.; Hann, S.; Fjeldsted, J. C. An Interlaboratory Evaluation of Drift Tube Ion Mobility-Mass Spectrometry Collision Cross Section Measurements. *Anal. Chem.* **2017**, *89* (17), 9048−9055.
(36) Feuerstein, M. L.; Kurulugama, R. T.; Hann, S.; Causon, T. Novel Acquisition Strategies for Metabolomics Using Drift Tube Ion Mobility-Quadrupole Resolved All Ions Time-of-Flight Mass Spectrometry (IM-QRAI-TOFMS). *Anal. Chim. Acta* **2021**, *1163*, 338508.
(37) Becker, C.; Fernandez-Lima, F. A.; Gillig, K. J.; Russell, W. K.; Cologna, S. M.; Russell, D. H. A Novel Approach to Collision-Induced Dissociation (CID) for Ion Mobility-Mass Spectrometry Experiments. *J. Am. Soc. Mass Spectrom.* **2009**, *20* (6), 907−914.
(38) Baker, E. S.; Tang, K.; Danielson, W. F.; Prior, D. C.; Smith, R. D. Simultaneous Fragmentation of Multiple Ions Using IMS Drift Time Dependent Collision Energies. *J. Am. Soc. Mass Spectrom.* **2008**, *19* (3), 411−419.
(39) Gao, X.; Zhang, Q.; Meng, D.; Isaac, G.; Zhao, R.; Fillmore, T. L.; Chu, R. K.; Zhou, J.; Tang, K.; Hu, Z.; Moore, R. J.; Smith, R. D.; Katze, M. G.; Metz, T. O. A Reversed-Phase Capillary Ultra-Performance Liquid Chromatography−Mass Spectrometry (UPLC-MS) Method for Comprehensive Top-down/Bottom-up Lipid Profiling. *Anal. Bioanal. Chem.* **2012**, *402* (9), 2923−2933.
(40) Adams, K. J.; Pratt, B.; Bose, N.; Dubois, L. G.; St. John-Williams, L.; Perrott, K. M.; Ky, K.; Kapahi, P.; Sharma, V.; MacCoss, M. J.; Moseley, M. A.; Colton, C. A.; MacLean, B. X.; Schilling, B.; Thompson, J. W. Skyline for Small Molecules: A Unifying Software Package for Quantitative Metabolomics. *J. Proteome Res.* **2020**, *19* (4), 1447−1458.
(41) MacLean, B. X.; Pratt, B. S.; Egertson, J. D.; MacCoss, M. J.; Smith, R. D.; Baker, E. S. Using Skyline to Analyze Data-Containing Liquid Chromatography, Ion Mobility Spectrometry, and Mass Spectrometry Dimensions. *J. Am. Soc. Mass Spectrom.* **2018**, *29* (11), 2182−2188.
(42) Stratton, K. G.; Webb-Robertson, B. M.; McCue, L. A.; Stanfill, B.; Claborne, D.; Godinez, I.; Johansen, T.; Thompson, A. M.; Burnum-Johnson, K. E.; Waters, K. M.; Bramer, L. M. PmartR: Quality Control and Statistics for Mass Spectrometry-Based Biological Data. *J. Proteome Res.* **2019**, *18* (3), 1418−1425.
(43) Chong, J.; Soufan, O.; Li, C.; Caraus, I.; Li, S.; Bourque, G.; Wishart, D. S.; Xia, J. MetaboAnalyst 4.0: Towards More Transparent and Integrative Metabolomics Analysis. *Nucleic Acids Res.* **2018**, *46* (W1), W486−W494.
(44) Odenkirk, M. T.; Zin, P. P. K.; Ash, J. R.; Reif, D. M.; Fourches, D.; Baker, E. S. Structural-Based Connectivity and Omic Phenotype Evaluations (SCOPE): A Cheminformatics Toolbox for Investigating Lipidomic Changes in Complex Systems. *Analyst* **2020**, *145* (22), 7197−7209.
(45) Guha, R. Chemical Informatics Functionality in R. *J. Stat. Soft.* **2007**, *18* (5), 1−16.
(46) Schliep, K.; Potts, A. J.; Morrison, D. A.; Grimm, G. W. Intertwining Phylogenetic Trees and Networks. *Methods Ecol. Evol.* **2017**, *8* (10), 1212−1220.
(47) Schliep, K. P. Phangorn: Phylogenetic Analysis in R. *Bioinformatics* **2011**, *27* (4), 592−593.
(48) Yu, G. Using Ggtree to Visualize Data on Tree-Like Structures. *Curr. Protoc. Bioinforma.* **2020**, *69* (1), e96.
(49) Kolde, R. *pheatmap: Pretty Heatmaps*; 2015. https://cran.r-project.org/web/packages/pheatmap/index.html.
(50) Fitzner, D.; Bader, J. M.; Penkert, H.; Bergner, C. G.; Su, M.; Weil, M.-T.; Surma, M. A.; Mann, M.; Klose, C.; Simons, M. Cell-Type- and Brain-Region-Resolved Mouse Brain Lipidome. *Cell Rep.* **2020**, *32* (11), 108132.
(51) Reis, A.; Rudnitskaya, A.; Blackburn, G. J.; Fauzi, N. M.; Pitt, A. R.; Spickett, C. M. A Comparison of Five Lipid Extraction Solvent Systems for Lipidomic Studies of Human LDL. *J. Lipid Res.* **2013**, *54* (7), 1812−1824.
(52) Massart, J.; Zierath, J. R.; Chibalin, A. V. A Simple and Rapid Method to Characterize Lipid Fate in Skeletal Muscle. *BMC Res. Notes* **2014**, *7* (1), 391.
(53) Odenkirk, M. T.; Stratton, K. G.; Gritsenko, M. A.; Bramer, L. M.; Webb-Robertson, B.-J. M.; Bloodsworth, K. J.; Weitz, K. K.; Lipton, A. K.; Monroe, M. E.; Ash, J. R.; Fourches, D.; Taylor, B. D.; Burnum-Johnson, K. E.; Baker, E. S. Unveiling Molecular Signatures of Preeclampsia and Gestational Diabetes Mellitus with Multi-Omics and Innovative Cheminformatics Visualization Tools. *Mol. Omi.* **2020**, *16* (6), 521−532.
(54) Eberlin, L. S.; Ifa, D. R.; Wu, C.; Cooks, R. G. Three-Dimensional Vizualization of Mouse Brain by Lipid Analysis Using Ambient Ionization Mass Spectrometry. *Angew. Chem., Int. Ed.* **2010**, *49* (5), 873−876.
(55) Murphy, R. C. *Mass Spectrometry of Lipids*; Springer, 1993.
(56) Cai, S.-S.; Syage, J. A. Comparison of Atmospheric Pressure Photoionization, Atmospheric Pressure Chemical Ionization, and Electrospray Ionization Mass Spectrometry for Analysis of Lipids. *Anal. Chem.* **2006**, *78* (4), 1191−1199.
(57) Liput, D. J.; Tsakalozou, E.; Hammell, D. C.; Paudel, K. S.; Nixon, K.; Stinchcomb, A. L. Quantification of Anandamide, Oleoylethanolamide and Palmitoylethanolamide in Rodent Brain Tissue Using High Performance Liquid Chromatography−Electrospray Mass Spectroscopy. *J. Pharm. Anal.* **2014**, *4* (4), 234−241.
(58) Xu, F.; Dang, Q.; Dai, X.; Fang, X.; Wang, Y.; Ding, L.; Ding, C.-F. Characteristics of Ion Activation and Collision Induced Dissociation Using Digital Ion Trap Technology. *J. Am. Soc. Mass Spectrom.* **2016**, *27* (8), 1351−1356.
(59) Dodds, J. N.; May, J. C.; McLean, J. A. Correlating Resolving Power, Resolution, and Collision Cross Section: Unifying Cross-Platform Assessment of Separation Efficiency in Ion Mobility Spectrometry. *Anal. Chem.* **2017**, *89* (22), 12176−12184.

https://doi.org/10.1021/acsmeasuresciau.1c00035
ACS Meas. Sci. Au 2022, 2, 67−75